ARTICLE

TECHNOLOGY

Brain-on-a-chip microsystem for investigating traumatic brain injury: Axon diameter and mitochondrial membrane changes play a significant role in axonal response to strain injuries

Jean-Pierre Dollé[1], Barclay Morrison III[2], Rene S. Schloss[1] & Martin L. Yarmush[1,3]

Diffuse axonal injury (DAI) is a devastating consequence of traumatic brain injury, resulting in significant axon and neuronal degeneration. Currently, therapeutic options are limited. Using our brain-on-a-chip device, we evaluated axonal responses to DAI. We observed that axonal diameter plays a significant role in response to strain injury, which correlated to delayed elasticity and inversely correlated to axonal beading and axonal degeneration. When changes in mitochondrial membrane potential (MMP) were monitored an applied strain injury threshold was noted, below which delayed hyperpolarization was observed and above which immediate depolarization occurred. When the NHE-1 inhibitor EIPA was administered before injury, inhibition in both hyperpolarization and depolarization occurred along with axonal degeneration. Therefore, axonal diameter plays a significant role in strain injury and our brain-on-a-chip technology can be used both to understand the biochemical consequences of DAI and screen for potential therapeutic agents.

INNOVATION

We previously described a strain injury model that maintains the three dimensional cell architecture and neuronal networks found *in vivo* and can be used to visualize individual axons and their responses to mechanical injury. The current studies utilized this technology to characterize axonal responses to uniaxial strains between two organotypic slices. This innovative approach was used to characterize the biochemical changes that are induced by DAI, and to test a novel therapeutic candidate, EIPA. Our brain-on-a-chip technology can be used for high-throughput screens of potential agents to ameliorate the consequences of DAI, which often accompanies traumatic brain injury (TBI).

INTRODUCTION

As many as half of hospital-admitted TBI patients experience events associated with diffuse axonal injury (DAI), making it the most common form of TBI[1]. This form of injury primarily results from catastrophic axonal strain due to inertial forces that occur during rapid rotation of the brain[2]. The initial physical trauma results in a primary injury that initiates a cascade of secondary injury responses and associated biological cascades.

The result of the primary injury is a breakdown in the axonal cytoskeleton, in particular microtubules[3]. This results in delayed axonal recovery, due probably to cytoskeletal reorganization, and a slow return to their original length results in undulations along the length of the axon. Since the majority of axonal transport occurs along microtubules, this breakdown results in the interruption in transport of vital proteins and organelles to distal sections of the axon and ultimately the accumulation of transport products producing axonal swellings that are hallmarks of DAI observed both *in vivo* and *in vitro*[3–6]. Since the strain injury is experienced along significant portions of an axon, multiple discrete disruptions in microtubules occur, resulting in numerous axonal swellings along the length of a given axon[7].

The response of axons to injury is highly complex with a multitude of variables playing a role. The caliber of the axon is one such variable, with *in vivo* injury models showing that small caliber axons are more susceptible to injury than larger caliber axons[8]. Smaller caliber axons, with fewer microtubules, are structurally weaker than larger caliber axons[9–11], but they also have a large surface-to-volume ratio and hence a reduced capacity to buffer calcium influx and exclude potential pathological molecules following injury[12–14]. Thus one of the objectives of the present study was to quantify the effect that axon caliber has on the injury response to different strain injuries.

Often, the end result of axonal strain injury is axonal degeneration[3] due to a combination of the primary injury, i.e. microtubule damage leading to axonal transport interruptions, and secondary injury mechanisms, i.e. influx of calcium and glutamate among others[15]. An increase in intracellular calcium following a strain injury is a well established response and can be responsible for initiating numerous downstream cell death cascades[15,16]. In addition to the production of adenosine triphosphate (ATP), mitochondria function to buffer intracellular calcium concentrations and are thus highly affected following strain injury[17].

[1] Department of Biomedical Engineering, Rutgers, The State University of New Jersey, 599 Taylor Road, Piscataway, New Jersey 08854, USA. [2] Department of Biomedical Engineering, Columbia University, 351 Engineering Terrace, 1210 Amsterdam Avenue, New York, NY 10027, USA. [3] Center for Engineering in Medicine, Massachusetts General Hospital/Harvard Medical School, Boston, MA 02114. Correspondence should be addressed to M.L.Y. (ireis@sbi.org).

Received 2 December 2013; accepted 5 March 2014; published online 19 May 2014; doi:10.1142/S2339547814500095

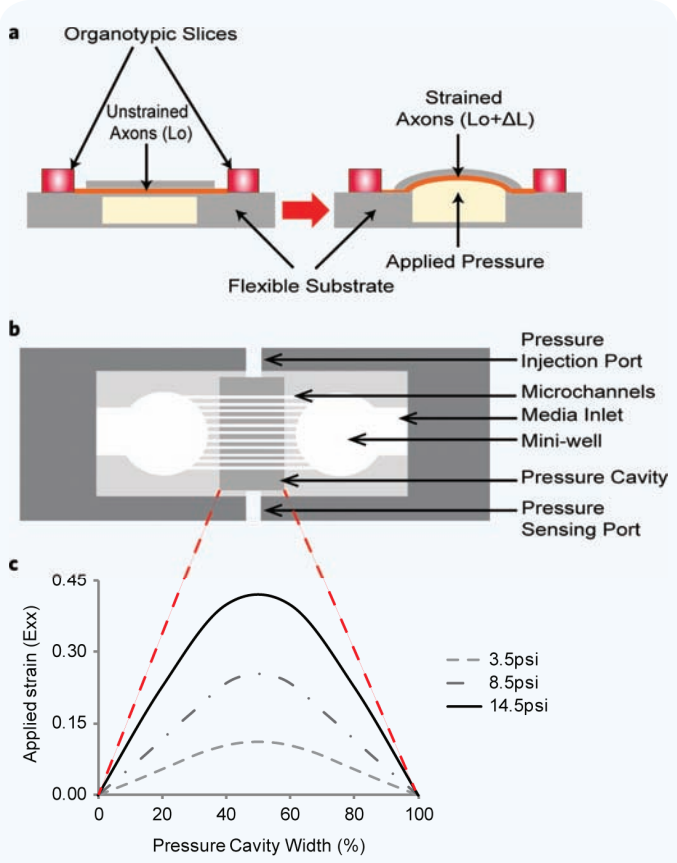

Figure 1 Organotypic uniaxial axonal strain device. (**a**) Schematic of device before and after strain application. (**b**) Detailed top view of assembled device. (**c**) Strain profile (E_{xx}) across the pressure cavity width. **a** and **b** are not to scale.

Excessive influx of calcium into mitochondria following injury can lead to the opening of the mitochondrial permeability transition pore (mPTP), i.e. the opening of a non-selective channel that allows solutes less than 1500 dalton to pass through[17]. This opening allows protons to freely flow across the inner mitochondrial membrane resulting in depolarization of the mitochondrial membrane potential (MMP)[18]. MMP is a key indicator of mitochondrial function and can be used to assess potential mechanisms that play a role in axonal dysfunction and degeneration[17,19]. Most studies examine mitochondrial changes within the cell body following injury. However, despite the fact that the axon sustains a great deal of damage, the response at the axonal level is not well understood. We previously described our brain-on-a-chip technology that can uniquely separate cell soma and individual axon responses. Our initial studies characterized the effect of strain on axonal morphology and cytoskeletal changes[20]. The model we used in our studies incorporates the connection and communication that occurs between two organotypic hippocampal slice cultures. Thus specific physiologically relevant pathways and networks may be studied, and depending on the orientation of the slices, or choice of slices (i.e. hippocampus-hippocampus or hippocampus-cortex) different pathways could be targeted for injury and injury responses assessed.

In the present study we report the response of hippocampal axons to increasing degrees of uniaxial strain injury with respect to axonal bead formation, delayed structural recovery and microtubule degeneration and demonstrate that their response to injury is further dependent on axonal diameter. Using our technology we are able to observe changes in MMP at the individual mitochondrial level within individual and bundles of axons. By monitoring and modulating axonal MMP, the extent of mitochondrial involvement in axonal degeneration could be assessed.

We also reveal a threshold that exists in applied strain injury on axonal MMP response, where at lower applied strains hyperpolarization occurs whereas at higher applied strains depolarization occurs. There is unfortunately no current "standard treatment" protocol for these secondary TBI effects and with almost one third of all injury related deaths in the United States attributed to a TBI related incident, finding relevant therapies is of utmost importance[21]. We therefore demonstrate that the Na^+/H^+ Exchange (NHE-1) inhibitor ethylisopropyl amiloride (EIPA) significantly attenuates these changes in mitochondrial membrane potential (MMP) and resultant axonal degeneration thus revealing a potential new DAI therapeutic.

RESULTS

Axonal bead formation following strain injury

In order to better understand the response of axons to the dynamic nature of a strain injury, we quantified axonal beading according to a number of different applied strain injuries. Using our strain injury model, the effects of three different uniaxial strains, i.e. 10%, 25% and 45%, were investigated in this study. These strains were selected since they represent the low, medium and high end of strains that have been shown to produce damage during TBI events[22–24].

An example of an axon that has formed a number of beads along its length within 4 hours of a uniaxial strain injury of 45% is shown in **Fig. 2a**. These beads occur at multiple points along the axon after injury and appear in the form of dense dark round structures. The number of these beads that occur along the length of an axon within 4 hours of injury was summed and normalized to 100 μm lengths for each applied strain (**Fig. 2b**). As expected, the number of axonal beads occurring along the length of the axon increases as the degree of applied strain is increased.

The dependence of axon/bundle diameter on bead formation following strain injury

In addition to quantifying the variation in number of beads with respect to the applied strain, we investigated the effect that axon/bundle diameter has on this response. It appears that the diameter of the axon/bundle plays a significant role in the response to the injury with respect to the number of beads that form (**Fig. 2c**). By grouping axon/bundle diameters into 0.4 μm groups a trend emerges. For all three applied strains the lowest diameter group produces the largest number of beads. As the axon/bundle diameter increases, the number of beads forming along the length decreases. For applied strains of 10 and 25%, no beading was observed on diameters above 1.8 μm and 2.2 μm respectively.

Axonal delayed elasticity following strain injury

When axons are subjected to high rates of strain they are known to temporarily form undulations along the length of the axon[20,25] (**Fig. 3a**). These undulations occur at multiple points along the axon length with varying amplitudes and result in localized increases in axonal length that when added, results in an overall increase in axon length as compared to the original length before injury. The axons that undergo this delayed elastic response recover to their original length generally within the hour[20,25]. These temporary increases in length were quantified for 10%, 25% and 45% applied strains (**Fig. 3b**). An increase in applied strain corresponded to an increase in this temporary elongation, i.e. ~2%, ~4.5% and ~9%.

The dependence of axon/bundle diameter on delayed elasticity following strain injury

We again quantified how the diameter of the axon/bundle affects the delayed elastic response to the applied strain. As observed with axonal beading, the axon diameter appears to have a significant effect on its response

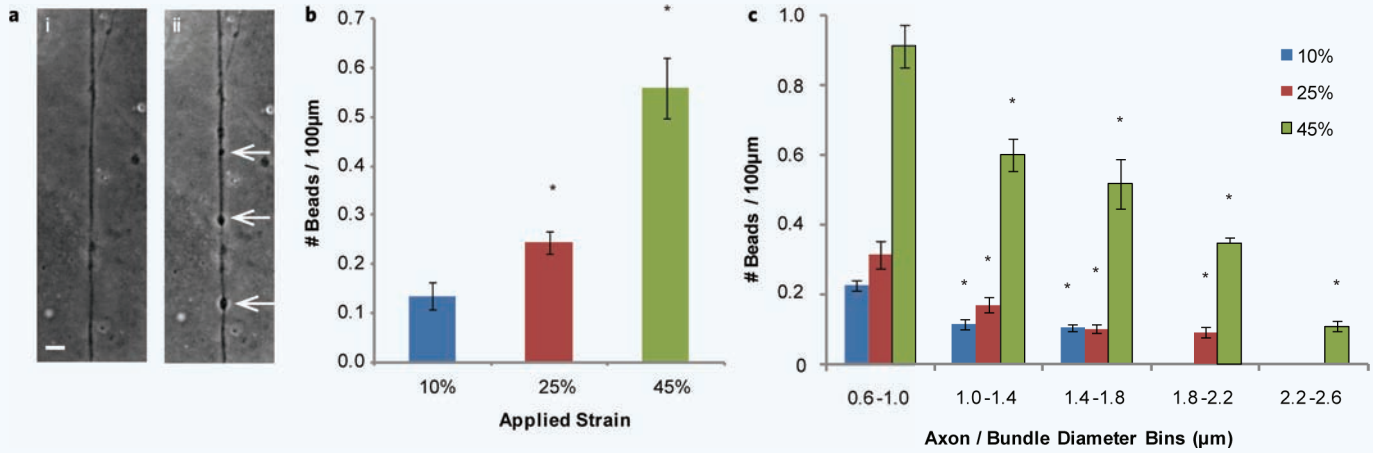

Figure 2 Uniaxial strain injury induced axonal beading. (**a**) Example of axonal beading (arrows) observed after uniaxial strain injury, (i) before injury and (ii) 4 hours after 45% strain injury. (**b**) The number of beads occurring along the length of an axon within 4 hours after injury normalized per 100 µm length for 10%, 25% and 45% applied strain. *P < 0.05 compared to 10% strain. (**c**) Diameter dependence of axonal beading after 10%, 25% and 45% uniaxial strain injury. The diameters of axons were grouped into 0.4 µm bins from 0.6 µm to 2.6 µm and the number of beads occurring along the length of an axon is normalized per 100 µm length. *P < 0.05 compared to 0.6 µm–1.0 µm for each specific applied strain. All error bars represent s.e.m. (number of experiments = 6–10). Scale bar, 10 µm.

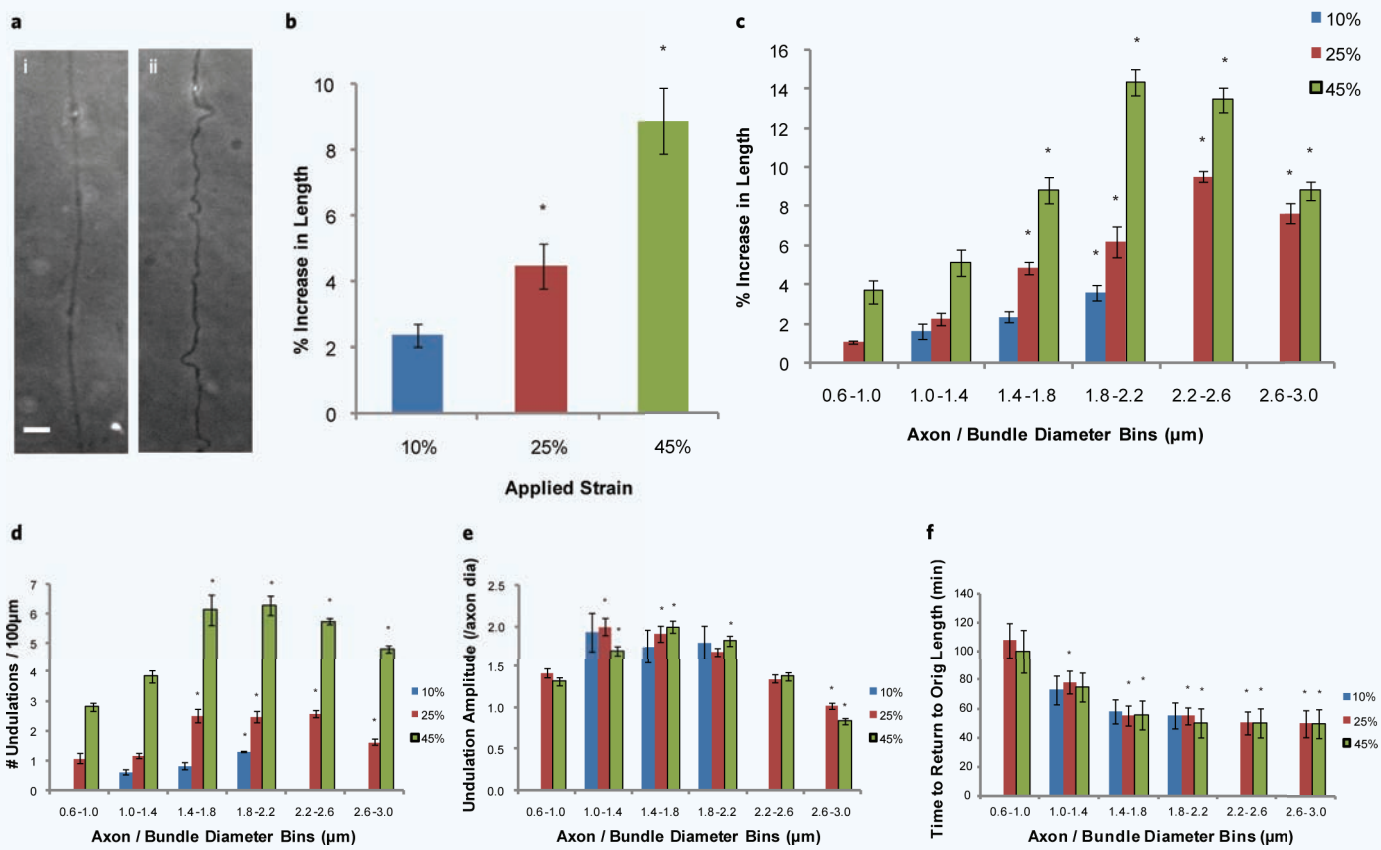

Figure 3 Increase in axon length following uniaxial strain injury. (**a**) Example of undulations following a 45% strain injury, (i) before injury and (ii) immediately after injury. (**b**) Increase in axon length due to strain for 10%, 25% and 45% applied strains. *P < 0.05 compared to 10% strain (number of experiments = 9). (**c**) The effect of different diameters on the increase in axon length following a 10%, 25% and 45% uniaxial strain injury. The diameters of axons were grouped into 0.4 µm bins from 0.6 µm to 3.0 µm. (**d**) The number of undulations observed along the axon length per 100 µm after 10%, 25% and 45% uniaxial strain injury. (**e**) The amplitude of undulations occuring along the length of the axon (normalized to the axon diameter before injury) after 10%, 25% and 45% uniaxial strain injury. (**f**) The time taken for axons to return to their original pre injury length after 10%, 25% and 45% uniaxial strian injury. *P < 0.05 compared to 0.6 µm–1.0 µm for **c** to **f** (number of experiments = 9). Scale bar, 10 µm.

to an applied strain injury. **Figure 3c–f** show that diameter affects different parameters within this delayed elastic effect, namely the temporary increase in axonal length, the number of undulations along the length of the axon (normalized to 100 μm), the amplitude of these undulations (normalized to the axon diameter before injury) and the time taken to return to the axon's original length. At the lower 10% applied strain, only axons between 1 μm and 2 μm experience this delayed elastic effect whereas for 25% and 45% applied strains, we observe increases in length throughout the range of diameters (**Fig. 3c**). For all three applied strains we observe clearly that the temporary increase in axon length following injury increases as axon diameter increases. For 25% and 45% applied strains we observe peaks in the region of 1.8 μm–2.6 μm. We next looked at how the number of undulations that occur along the length of the axon varies with axon diameter (**Fig. 3d**). We observe diameter dependence at the lower end of axon diameters; however a plateau appears around 1.4 μm in diameter with a slight drop-off at the higher diameters. The amplitude of these undulations (**Fig. 3e**) generally did not rely as heavily on the diameter as the other two parameters shown, although at the higher end of the diameter spectrum there was a drop-off. As axon / bundle diameter increased so the time taken to return to the axons' original length decreased. For diameters above 1.4 μm, axons returned to their original length within 50 minutes, with the axons below 1 μm taking as long as ~105 minutes (**Fig. 3f**).

Axonal degeneration assessed following strain injury

The breakdown in microtubules and axonal transport can ultimately lead to axonal degeneration since distal portions of the axon do not receive necessary nutrients to sustain cell function[26]. Evidence of this can be seen in **Supplementary Fig. 1a–d** showing how, with respect to applied strain and time following injury, microtubules within the axon breakdown (through staining of β-tubulin). Microtubule degeneration can be observed through the increase in both the number and size of gaps in fluorescence as both strain and time following injury is increased. Degeneration is observed as early as 1 hour post injury at the higher 45% applied strain. Confirmation of a breakdown in axonal transport can be visualized by an accumulation in certain transported proteins, namely the protein amyloid-β precursor protein (APP)[27]. **Supplementary Fig. 1e–h** shows APP staining in axons subjected to increasing strains and at various time points following injury. There is generally an increase in the number and size of these APP accumulations over time.

Thus when axonal degeneration is assessed at 24 hours post strain injury, with respect to the three different applied strains, we see a proportional increase in degeneration (**Fig. 4a**). The applied strains of 10% and 45% seem to represent the two ends of the spectrum, with 10% applied strain experiencing relatively minimal degeneration and 45% applied strain experiencing almost complete degeneration. Of the axons

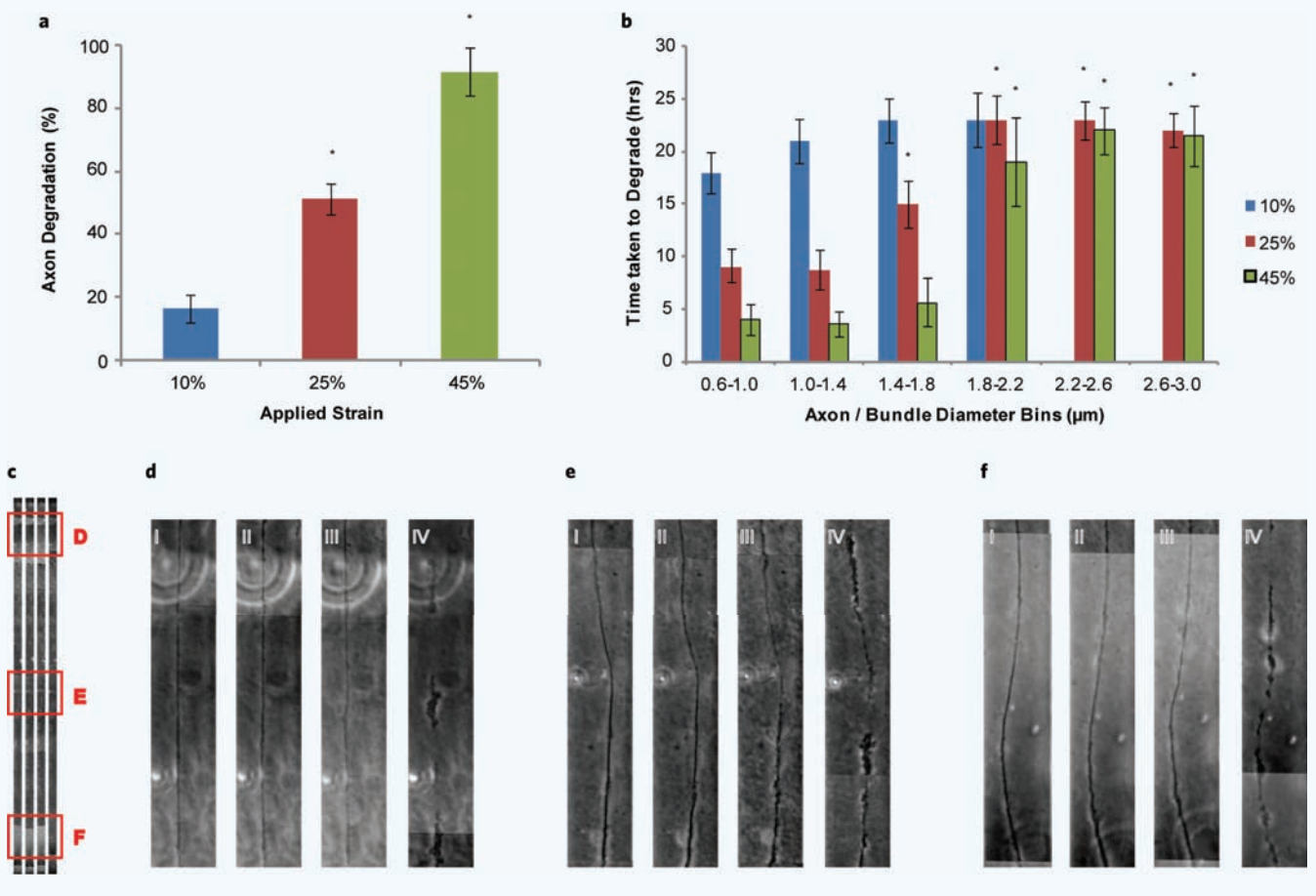

Figure 4 Axonal degradation following a uniaxial strain injury. (**a**) Axonal degradation was assessed at 24 hours following uniaxial strain injury with respect to 10%, 25% and 45% applied strain. *P < 0.05 compared to 10% strain (number of experiments = 12). (**b**) The time taken to degrade was monitored with respect to axon diameter. The diameters of axons were grouped into 0.4 μm bins from 0.6 μm to 3.0 μm. *P < 0.05 compared to 0.6 μm–1.0 μm (number of experiments = 12). (**c**) An example of an axon along the full length of the strain region undergoing degradation over time. Three different positions are highlighted and shown in higher magnification in **d–f**. Position **d** and **f** correspond to the regions of lowest strain and **e** the region of highest strain. (**d–f**) (i) axon before injury, (ii) axon immediately following injury, (iii) 18 hours post injury and (iv) 20 hours post injury.

that undergo degeneration, it appears that axonal/bundle diameter again has an effect, this time with respect to the time taken to degrade (**Fig. 4b**). In general, the time to degrade increased as diameter increased. When a 10% strain was applied, the majority of degeneration occurs within 24 hours. When a 25% strain was applied, the smaller diameter axons (0.6–1.4 μm) degrade within 10 hours increasing to within 24 hours at the higher diameters (1.8–3.0 μm). At 45% applied strain a similar trend is observed just at a more accelerated rate, where at small diameters (0.6–1.8 μm) degeneration is observed within 5 hours again increasing to 24 hours for the larger diameters (1.8–3.0 μm).

The majority of axon degeneration due to a uniaxial strain injury is preceded by axonal undulations and/or beading, however this is not always the case. **Figure 4c–f** highlight three different positions along the length of an axon and how it degrades over time. **Figure 4d,e,f (i) and (ii)** show an axon before and immediately after injury indicating no undulations, however in this particular example, by 18 hours [**Fig. 4d,e,f (iii)**] we observe the beginnings of degeneration and by 20 hours [**Fig. 4d,e,f (iv)**] significant membrane breakdown has occurred.

Changes in mitochondrial membrane potential (MMP) following strain injury

Another indicator of axonal health is monitoring the changes in MMP[17,19]. This was done by observing changes in MMP (using JC-1 dye) at discrete positions along the length of the axon over 24 hours. To initially assess the stability of JC-1 and MMP over a 24-hour period, control experiments were performed where the device simulated a sham injury (**Fig. 5a**). Very little change in MMP is observed over a 24-hour period. A controlled depolarization was performed by adding 10 μm of FCCP to the cultures resulting in a decrease in MMP to approximately 11% of the original fluorescence (**Fig. 5a**). When a 10% strain is applied (**Fig. 5b**) we initially see no significant change in membrane potential immediately following injury (0 hour), which is consistent along the full length of the microchannel. Over the first 4 hours following injury we observe increases in MMP particularly at the two ends of the pressure cavity, i.e. in the regions of low applied strain (positions 1–3 and 9–11). In the central region (positions 4–8 — corresponding to the region in which maximal strain is experienced (**Fig. 1c**)), we observe a significant increase in MMP occurring between 4 and 24 hours, with a peak around a 3-fold increase in MMP. When a 25% strain is applied (**Fig. 5c**) an overall similar trend is observed, where slight increases are observed over the initial 4 hours following injury followed by significant increases in MMP in the central strain region. By 24 hours post injury the increase in fluorescence ratio is around 4-fold the membrane potential observed before injury. When a 45% strain is applied (**Fig. 5d**), we appear to have exceeded a threshold of injury where we observe a dramatic decrease in membrane potential. The region of maximal decrease again corresponds to the central region where maximal strain is experienced. This decrease is observed immediately following injury with further incremental decreases observed until 24-hours after injury. Representative images of changes in JC-1 fluorescence along the length of the microchannel before injury and 24 hours following injury for 10%, 25% and 45% applied strain can be seen in **Supplementary Fig. 2**.

Change in mitochondrial numbers along axon

The JC-1 dye was also used to monitor mitochondrial numbers along the length of the axon. It is interesting to note, that there was an increase in the number of mitochondria observed for the 25% applied strain condition (**Supplementary Table 1**). This was the only condition that a significant increase in the number of mitochondria was observed as compared to before injury, i.e. a ~2.1-fold increase in the center increasing to over 3-fold at the edges of the cavity. This increase profile was the inverse of changes observed with changes in MMP. Representative images showing the increase in number of mitochondria using JC-1 fluorescence can be seen in **Supplementary Fig. 2b (i) and (ii)**.

MMP hyper/depolarization attenuated through the addition of EIPA and CsA

Sodium-hydrogen exchange (NHE1) inhibitors have been shown to reduce the influx of calcium into mitochondria, inhibit the mPTP and preserve the MMP after injury[28,29]. We applied the NHE1 inhibitor ethylisopropyl amiloride (EIPA) in this study and its effect on MMP was evaluated (**Fig. 5e–g**). The effects of EIPA were compared to the well-studied mPTP inhibitor cyclosporine A (CsA) (**Supplementary Fig. 3**).

When a 10% strain was applied to axons pretreated with EIPA (**Fig. 5e**), we observed an almost complete inhibition of MMP hyperpolarization as compared to the untreated condition (**Fig. 5b**) (the peak increase in MMP was 1.18-fold). When a 25% strain was applied (**Fig. 5f**) we again observed an inhibition on MMP hyperpolarization, however not to the extent as that seen in the 10% strain condition (peak increase in MMP was 2.4-fold). The peak increase in MMP was again observed in the central region of the device, with a flatter arc. When a 45% strain was applied (**Fig. 5g**), we observed no significant change in membrane potential immediately following injury, which was dramatically different to the large drop off in membrane potential observed in untreated conditions (**Fig. 5d**). There was a steady drop in MMP over a 24-hour period (peak decrease in MMP was ~0.87-fold). Representative images of changes in JC-1 fluorescence after the application of EIPA before injury and 24 hours following injury for 10%, 25% and 45% applied strain can be seen in **Supplementary Fig. 4**.

We applied CsA prior to injury and monitored changes in MMP. When a 10% strain was applied to axons pretreated with CsA, we observed a complete inhibition of MMP hyperpolarization (**Supplementary Fig. 3a**) as compared to untreated conditions (**Fig. 5b**) and similar to that seen in EIPA treated conditions (**Fig. 5e**). The peak increase in MMP was 1.05-fold within 2 hours going back to ~1 by 24 hours. When a 25% strain was applied (**Supplementary Fig. 3b**), we again observed a complete inhibition on MMP hyperpolarization as compared to untreated conditions (**Fig. 5c**) and to EIPA treated conditions (**Fig. 5f**). The peak increase in MMP was ~1.05-fold immediately following injury, decreasing to ~1 by 4 hours and then increasing back to ~1.05-fold by 24 hours (however not statistically significant). When a 45% strain was applied (**Supplementary Fig. 3c**), we observed an inhibition in MMP depolarization immediately following strain injury as compared to untreated conditions (**Fig. 5d**), however not as complete an inhibition as that observed in EIPA treated conditions (**Fig. 5g**). The immediate drop in MMP peaks around 0.87-fold in the central region of the device steadily decreasing over 24 hours to peak around 0.83-fold.

EIPA and CsA attenuate axonal degeneration assessed following strain injury

We showed that pretreating axons with EIPA and CsA before strain injury attenuates both hyperpolarization at 15% and 25% applied strains and depolarization at 45% applied strain (**Fig. 5e–g, Supplementary Fig. 3**). We next assessed how this MMP inhibition translates to overall axonal health by observing axonal degeneration 24 hours post injury (**Fig. 6**). For the 10% applied strain we observed no significant change in degeneration from both the EIPA and CsA treated conditions. However for both the 25% and 45% applied strain conditions, we observe significant decreases in axonal degeneration for both the EIPA and CsA treated conditions, with no significance between EIPA and CsA treated conditions.

DISCUSSION

We have designed and tested the biochemical consequences of DAI using our brain-on-a-chip technology. The results of our studies demonstrate: (1) the significance that axonal diameter plays in response to an applied strain injury, (2) a distinct threshold in MMP exists with respect to applied strain injury and controlling changes in MMP can play a significant role in axonal degeneration and (3) our device can be used to screen potential therapeutic candidates.

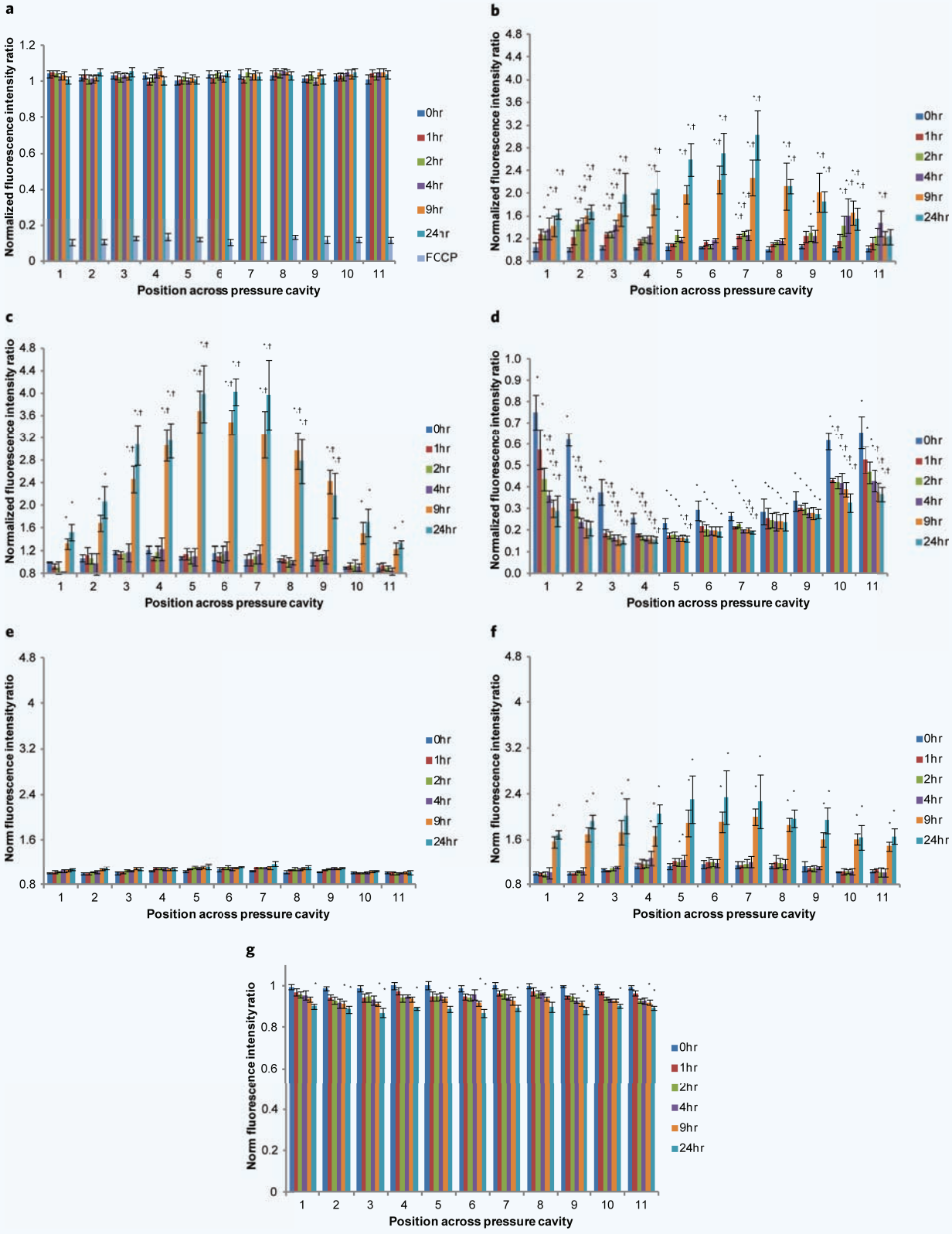

Figure 5 Monitoring MMP changes over a 24-hour period following uniaxial strain injury. MMP changes are normalized to their potential before injury and assessed at 11 discrete sections along the axons and 6 time points, i.e. immediately following injury (0 hour), 1 hour, 2 hours, 4 hours, 9 hours and 24 hours post injury. (**a**) Uninjured control and addition of mitochondrial uncoupler FCCP. Changes in MMP after applying a uniaxial strain injury, (**b**) 10% applied strain, (**c**) 25% applied strain and (**d**) 45% applied strain. MMP changes were assessed after application of the NHE-1 inhibitor EIPA and uniaxial strain injuries. (**e**) EIPA and 10% applied strain, (**f**) EIPA and 25% applied strain and (**g**) EIPA and 45% applied strain. *$P < 0.05$ compared to MMP at that particular position before injury. †$P < 0.05$ compared to MMP at that particular time point at positions 1 and 11 (number of experiments = 8).

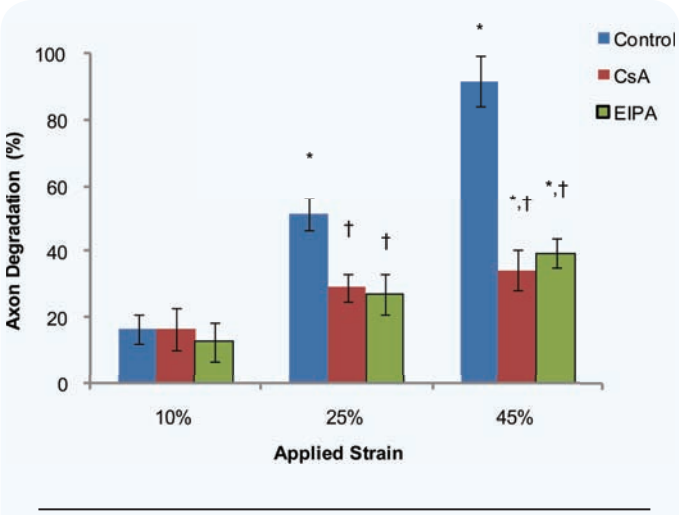

Figure 6 Axonal degradation assessed at 24 hours following uniaxial strain injury after treatment with EIPA and CsA. Degradation was assessed for three uniaxial strains, i.e. 10%, 25% and 45%. *$P < 0.05$ compared to 10% strain, †$P < 0.05$ compared to control (untreated) for that particular applied strain injury (number of experiments = 4–12).

As expected, when the applied strain was increased the morphological and structural response to injury generally increased. This included increases in axonal bead formation, delayed elasticity responses, microtubule degeneration, APP accumulation and ultimately increases in axonal degeneration. Not only does varying the applied strain dictate axonal response to injury but the diameter of the axon or axonal bundle appears to play a significant role in this response, i.e. as diameter increases the number of beads decreases. The number of microtubules found within an axon is dependent on the axon diameter, i.e. as the diameter of the axon increases so does the number of microtubules[30]. Therefore as the diameter of the axon or axon bundle increases there are more microtubules across which the load is distributed. Therefore a greater load distribution potentially results in fewer microtubules being damaged during injury and consequently fewer beads forming. Our results correspond to those observed *in vivo*, where using a fluid percussion injury model it was shown that smaller caliber axons are more susceptible to TBI[31].

The range of diameters observed in our model correlate with those detected *in vivo* in rat hippocampi (0.1 μm–2.8 μm, with average below 1 μm)[32]. We observe a large range of axon diameters within our microchannels that include both individual axons and bundles of axons (they clearly come together near the start of a microchannel and proceed to stay together for the duration of the channel). In this study we do not know if the larger bore axons observed are individual axons or bundles of axons, but confirmation will be done in further studies.

The undulations observed along the length of axons following high strain rate injuries (commonly termed "delayed elastic effect") has been shown to be due to the breakdown and subsequent misalignment in axonal microtubules following injury[3,25]. When this delayed response was quantified we observed temporary increases in axonal length that corresponded to the applied strain which may result in prolonged activation of mechanosensitive ion channels thus further exacerbating pathological responses[33,34]. This could explain the fact that along sections of axon where "delayed elasticity" was observed, there was both an increase in the number of axonal beads forming and an acceleration in time taken for axonal degeneration to occur.

In a bundle each axon is connected to an adjacent axon through integrin binding[35] so if microtubules in a particular axon are damaged and that particular axon undergoes the delayed elastic response observed, since it is bound to an adjacent axon it will affect both axons returning to their original length. This resistance to return to an axons original length seems to be fairly substantial since we and others observe that it takes a considerable time for an axon to return to its original length, generally within the hour[3,25]. Therefore, if only a few axons within a particular bundle are affected, it would have an effect on the whole bundle. This is probably why we observe an increase in the number of undulations and corresponding temporary increase in axon length as diameter increases. With that said, since not all microtubules are damaged during the initial injury[7], the larger the diameter, the more the undamaged microtubules there are to "pull" the axon back to its original length, thus we observe a decrease in time taken to return to original length as the diameter increases. These increases in length observed in our study are larger than those observed using other injury models[3,25]. However, they also state that they do not observe primary axotomy at strain levels below 65%, whereas in our model we observe primary axotomy occurring at 45% applied strain demonstrating differences in the models[20]. The majority of the degeneration observed in our model occurs within 24 hours after strain injury, and is consistent with other similar *in vitro* models[3]. This time frame is consistent with degeneration observed in *in vivo* TBI injury models and has been found to occur in just a few days in humans following injury[36–38].

Observing changes in mitochondrial function is one way to assess the health of a cell or axon, thus enabling one to assess potential mechanisms that play a role in axonal degeneration[17,19]. The MMP that exists across the mitochondrial inner-membrane among other things, controls ATP synthesis, mitochondrial calcium buffering and the generation of reactive oxygen species (ROS), all fundamental processes during normal mitochondrial function[39]. Disrupting any one of these functions can lead to cell death. Events resulting in MMP depolarization (can lead to a reduction in ATP and opening of the mPTP) or hyperpolarization (can lead to the generation of ROS), can lead to detrimental effects on the cell[40,41]. Our strain injury device highlights an applied strain threshold (25% < *strain threshold* > 45%), below which there is a delayed MMP hyperpolarization and above which an immediate and sustained depolarization.

MMP hyperpolarization has been shown to be an early indicator of apoptotic initiated cell death in T-cells, epithelial cells, and neurons[40,42,43]. This MMP hyperpolarization is most likely due to an inhibition in the electron transport chain, specifically inhibition of either/both F_0F_1-ATPase or adenine nucleotide translocase (ANT)[44]. Inhibition of F_0F_1-ATPase results in a buildup of hydrogen ions in the mitochondrial inner-membrane space resulting in an increase in MMP[45]. Inactivation of F_0F_1-ATPase has been shown to occur in a controlled cortical impact (CCI) model of TBI[46]. ANT is an ADP/ATP antiporter that exchanges ADP for ATP across the inner mitochondrial membrane (i.e. ADP^{3-} into the matrix and ATP^{4-} out, thus normally reducing part of the electrochemical gradient) therefore inhibiting this function results in an increase in the MMP[47]. The two main factors shown to inhibit ANT is Bax (shown to increase in response to a CCI injury[48]) and calcium (inhibition of ANT appears to be calcium concentration dependent, i.e. only at lower pathological concentrations[44]).

The 3- and 4-fold increases in MMP we observe at lower applied strain levels is similar to the 4-fold increase in MMP observed within three hours in D283 medulloblastoma cells and the 2-fold increase in MMP observed within 16 hours of rat hippocampal neurons exposed to staurosporine[40] (results in significant increases in both intracellular and mitochondrial calcium[49] as observed in uniaxial strain injury[16]). A 4-fold increase in JC-1 fluorescence intensity ratio equates to an increase in ~35 mV, i.e. using the Nernst equation for cationic indicators (where normal physiological inner membrane potential is approximately 150–180 mV)[39].

For applied strains above the threshold we observe MMP depolarization almost to the level seen after application of the uncoupler FCCP. This initial response threshold to strain injury is similar to results observed in an *in vitro* biaxial strain injury model where high strain injuries resulted

in a significant decrease in MMP within 15 minutes and maintained over 24 hours[50]. Decreases in MMP of >60% have also been observed in an *in vitro* fluid percussion injury[51]. The MMP threshold observed corresponds to calcium threshold concentrations observed within mitochondria, which when exceeded, result in the collapse of the MMP and an opening of the mPTP[52].

The shift of MMP from hyperpolarization to depolarization has been observed when isolated mitochondria from the cortex were exposed to various levels of calcium[44]. At low pathological levels of calcium a significant hyperpolarization was observed, whereas complete depolarization occurred at higher pathological calcium levels. We believe that we may be observing a calcium concentration dependent effect on MMP where at relatively low levels of applied strain (10% and 25%) hyperpolarization occurs whereas at higher levels of applied strain (45%) depolarization occurs due to opening of the mPTP.

Since mitochondrial health is a good indicator of overall cell well-being, we initially wanted to observe how changes in MMP correlate to axonal degeneration with respect to various applied strains. However, after observing the dramatic shifts in MMP we wanted to see how much of an influence stabilizing the MMP may have on overall axonal degeneration and therefore looked at molecules that could attenuate these effects. We looked to the NHE-1 inhibitor EIPA (sodium-hydrogen exchanger (NHE)) which is a counter-transport system that couples the extrusion of protons to the influx of sodium (regulating cell pH and volume)[53]. The reason for using EIPA was 3-fold, (1) it reduces the amount of protons entering the mitochondrial matrix thus potentially stabilizing MMP[54], (2) some NHE-1 inhibitors have been shown to decrease both intracellular and mitochondrial calcium[28] due to the fact that there is a reduction in sodium influx and therefore an inhibition of Na^+/Ca^{2+} channels and (3) certain NHE-1 inhibitors (HOE-642) have also been shown to inhibit mPTP opening[55]. The decrease in MMP hyperpolarization observed at the lower applied strains after EIPA was added is probably due to both a decrease in mitochondrial calcium and protons entering the matrix. With respect to the inhibition of MMP depolarization demonstrated by the addition of EIPA, this is likely due to a combination of a decrease in mitochondrial calcium and inhibition of the mPTP. This response appears to be better than the well-known mPTP inhibitor CsA[56].

As a result of attenuating both MMP hyperpolarization and depolarization, we show that EIPA results in a significant reduction in axonal degeneration revealing how considerable an effect mitochondrial health has on axonal degeneration and its use as a potential therapeutic for traumatic axonal strain injury.

Further studies should be done to investigate the therapeutic window in which EIPA could be administered following a strain injury. With the delayed response in significant changes in MMP observed for lower strains we believe that a window may exist, however for higher strains, that remains to be seen.

METHODS

Organotypic hippocampus slice isolation

All animal experiments were approved by the Animal Care and Use Committee of Rutgers, The State University of New Jersey and in accordance with protocols approved by the NIH guidelines for the care and use of laboratory animals. The brains of Sprague-Dawley rat pups (Taconic) between the ages of 4 to 6 days old were removed and placed in ice cold Gey's Balanced Salt Solution (Sigma) supplemented with 10 mM D-glucose (Sigma) and 3 μm Kynurenic Acid (Sigma). In our hands, we have found that axon extension from the periphery of organotypic hippocampal slices is very dependent on the age of the rat pup they have been excised from with axon extension decreasing significantly after day 6 (data not shown). The hippocampi were separated from the surrounding cortex and sliced into 400 μm thick slices using a McIllwain Tissue Chopper (Stoelting Co, IL). The slices were carefully placed into Polydimethylsiloxane (PDMS) (Sylgard 184, Fischer Scientific) mini-wells and orientated such that the dentate gyrus (DG) region was facing the CA3/CA1 region of the adjacent slice, i.e., these regions were facing the microchannel. The PDMS was precoated with poly-d-lysine (1 mg/ml, Sigma) and laminin (25 μg/ml, Sigma). The device was filled with enough serum containing media (1:1:2 of heat inactivated horse serum, Hanks Balanced Salt Solution, Basal Medium Eagle, supplemented with 0.5 mM L-Glutamine, 30 μg/ml gentamycin and 10 mM HEPES, all from Invitrogen) to cover the exposed basement PDMS area. The organotypic hippocampus slice cultures (OHC) were placed on a rocker (~1 revolution/60 s) in a humidified 5% CO_2, 37°C incubator. Glial cell proliferation was reduced by changing from serum containing media to a serum free media after 24 hours (Neurobasal A, B27, 0.5 mM L-glutamine, 30 μg/ml gentamycin and 10 mM HEPES, all from Invitrogen). Thereafter, half of the media was changed every 48 hours.

Strain device

Schematic representations of the strain device are shown in **Fig. 1. Figure 1a** depicts the overall functioning of the device where two organotypic slices are placed on a flexible substrate (PDMS). Over a 14-day period, axons extend from the periphery of the slice, and in general, enter the nearest PDMS microchannel (**Fig. 1b**)[20]. These axon extensions are guided down the PDMS microchannels where they eventually exit and connect to the adjacent hippocampal slice[20]. The microchannel dimensions used were 50 μm (microchannel width) × 6 μm (microchannel height) × 50 μm (microchannel spacing). Under the microchannel section of the device is a cavity, that when pressurized, deflects upwards causing the PDMS to strain in a uniaxial direction[20]. This pneumatic pressure is produced through coupling to a pressure injection system. The injected volume and rate of injection are varied to produce a variety of strains and rate of strain[20].

In order to protect the hippocampal slices and extending axons from fluid shear during device handling, mini-wells with a diameter of 3 mm were punched into the microchannel PDMS at a spacing of 2 mm from each other with a media access channel leading to each of the mini-wells. In order to reduce media evaporation, a semi-permeable membrane (permeable to O_2 and CO_2 but not permeable to H_2O, ALA Scientific Instruments) was placed over the device and sealed with an O-ring. Three different uniaxial strains were applied to axons extending through the microchannel sections, i.e. 10%, 25% and 45%. The time to reach maximum deflection for each of the three strains was kept constant at approximately 22 ms. The strain profiles across the pressure cavity are shown in **Fig. 1c** reflecting a maximum in the center of the cavity.

Imaging axons within microchannels

Microchannels (containing axons that connect the two hippocampal slices together) were selected for imaging and analysis based on the number of axons within a channel, and provided that there was no glial cell migration down the microchannel. Images were taken using a computer interfaced inverted Olympus IX81 DSU microscope (Olympus) controlled by Slidebook software (Olympus) using a 40X objective. Only the area within the pressurized section was imaged and analyzed. Each microchannel was split into 11 sections (the number of 40X objective images it took to traverse the pressurized area — each image was approximately 180 μm × 180 μm). Images were taken before applying a uniaxial strain injury, immediately after injury (0 hour), 1 hour, 2 hours, 4 hours, 9 hours and 24 hours post injury. When images were taken before injury, each position along every microchannel was saved in Slidebook and at every subsequent time point thereafter recalled and reimaged thus allowing for each position along the microchannel/axon to be compared over time.

Axonal beading analysis

Axons within a particular microchannel were analyzed for axonal beading after strain injury. Calculations were done on images taken before and 4 hours post injury. The criteria for beading were: (1) has to be at least twice the diameter than adjacent sections of the axon and (2) the beading has to grow in size for multiple time points (minimizes the inclusion of

transportation of large organelles down the length of the axon which may appear to be an injury induced bead). The beading is normalized to the length of the axon within the pressure cavity section, i.e. per 100 μm sections of axon length. The diameters of analyzed axons were measured at 10–15 discrete positions along the length of the axon and then averaged. Diameter dependence calculations were done by grouping axons into 0.4 μm diameter bins starting from 0.6 μm up to 2.6 μm (i.e. 0.6 μm–1.0 μm, 1.0 μm–1.4 μm, 1.4 μm–1.8 μm, 1.8 μm–2.2 μm and 2.2 μm–2.6 μm).

Delayed elasticity analysis

The increase in axon length following strain injury (i.e. the undulations that occur along the length of the axon immediately following strain injury), was measured and reported as a % increase. Measurements were done on images taken before and immediately following injury. The amplitude of these undulations were measured from the centerline of the axon before injury to the centerline of the axon post injury and normalized to the axon diameter. The diameters of analyzed axons were measured at 10–15 discrete positions along the length of the axon and then averaged. Diameter dependence calculations were done by grouping axons into 0.4 μm diameter bins starting from 0.6 μm up to 3.0 μm (i.e. 0.6 μm–1.0 μm, 1.0 μm–1.4 μm, 1.4 μm–1.8 μm, 1.8 μm–2.2 μm, 2.2 μm–2.6 μm and 2.6 μm–3.0 μm). The time taken for different diameter axons to return to their original length was noted.

Axonal degeneration analysis

Axonal degeneration was analyzed using 15–20 microchannels for a given strain experiment. Calculations were done using images taken before applying a uniaxial strain injury and 24 hours after injury. The numbers of axons entering and exiting a particular microchannel were counted before injury. If at any section along the length of the axon there is no longer a visible outline of an axon, and no mitochondrial activity (JC-1 fluorescence), this is seen as an axon that has undergone degeneration. This is normalized to the total number of axons and reported as a %. The time taken for different diameter axons to degrade was noted.

Monitoring changes in mitochondrial membrane potential

The changes in axonal MMP due to applied uniaxial strains were monitored using the JC-1 dye (5,5′,6,6′-tetrachloro-1,1′,3,3′-tetraethylbenzimidazoly lcarbocyanine iodide) (Invitrogen). This dye exhibits a fluorescence shift between green (~525 nm) and red (~590 nm) depending on the MMP. When mitochondria depolarize, the red aggregate color is replaced by diffuse green monomer fluorescence. Thus a depolarization is indicated by a decrease in the red/green fluorescence intensity ratio. A decrease in this fluorescence intensity ratio was thus interpreted as a decrease in MMP and an increase in this ratio an increase in MMP[57,58]. This ratio allows for comparing changes in MMP between different conditions and over time. The same exposure time was used for each filter in all experiments. Cultures were incubated with 2 mM JC-1 for 30 minutes in serum free media on a rocker at 37°C and 5% CO_2. This was followed by 2 washes in serum free media for 10 minutes each at 37°C and 5% CO_2. The cultures were allowed to equilibrate for a 90-minute period before taking initial images.

Between 15–20 microchannels were selected to be analyzed for a given strain experiment. Images were taken before applying a uniaxial strain injury, immediately after injury (0 hour), and 1 hour, 2 hours, 4 hours, 9 hours and 24 hours post injury. In order to account for any changes in MMP due to temperature changes during handling of the device (imaging or strain injury device attachment), uninjured controls were monitored over a 24 hour period. As a positive control, 10 μm of carbonyl cyanide p-(trifluoromethoxy) phenylhydrazone (FCCP) (Sigma) was added to cultures for 10 minutes for a controlled depolarization.

EIPA treated conditions

The sodium-hydrogen exchange inhibitor (NHE1) ethylisopropyl amiloride (EIPA) was applied in this study and its effect on MMP (through the use of JC-1) and axonal degeneration (24 hours post strain injury) along the length of the axon and over time were assessed. EIPA was administered at 10 μM in serum free media 30 minutes before strain injury until the end of the experiment.

Data analysis

Data are represented as indicated. One way analysis of variance (ANOVA) was used to determine statistical significance. Tukey post-hoc tests were used to determine differences between groups and $P < 0.05$ was regarded as significant.

ACKNOWLEDGEMENTS

This work was supported by grants from the New Jersey Commission for Brain Injury Research (BIR-1.08.016), the National Institute of Biomedical Imaging and Bioengineering (NIH P41 EB002503), and the National Institute of General Medical Sciences (Rutgers-UMDNJ Biotechnology Training Program: T32 GM008339).

REFERENCES

1. Meythaler, J.M., Peduzzi, J.D., Eleftheriou, E. & Novack, T.A. Current concepts: Diffuse axonal injury-associated traumatic brain injury. *Arch. Phys. Med. Rehabil.* **82**, 1461–1471 (2001).
2. Smith, D.H. & Meaney, D.F. Axonal damage in traumatic brain injury. *Neuroscientist* **6**, 483–495 (2000).
3. Tang-Schomer, M.D., Patel, A.R., Baas, P.W. & Smith, D.H. Mechanical breaking of microtubules in axons during dynamic stretch injury underlies delayed elasticity, microtubule disassembly, and axon degeneration. *FASEB J.* **24**, 1401–1410 (2010).
4. Gennarelli, T.A. *et al.* Axonal injury in the optic nerve: A model simulating diffuse axonal injury in the brain. *J. Neurosurg.* **71**, 244–253 (1989).
5. Kilinc, D., Gallo, G. & Barbee, K.A. Mechanically-induced membrane poration causes axonal beading and localized cytoskeletal damage. *Exp. Neurol.* **212**, 422–430 (2008).
6. Povlishock, J.T. & Christman, C.W. The pathobiology of traumatically induced axonal injury in animals and humans: A review of current thoughts. *J. Neurotrauma* **12**, 555–564 (1995).
7. Tang-Schomer, M.D., Johnson, V.E., Baas, P.W., Stewart, W. & Smith, D.H. Partial interruption of axonal transport due to microtubule breakage accounts for the formation of periodic varicosities after traumatic axonal injury. *Exp. Neurol.* **233**, 364–372 (2012).
8. Stone, J.R., Singleton, R.H. & Povlishock, J.T. Intra-axonal neurofilament compaction does not evoke local axonal swelling in all traumatically injured axons. *Exp. Neurol.* **172**, 320–331 (2001).
9. Friede, R.L. & Samorajski, T. Axon caliber related to neurofilaments and microtubules in sciatic nerve fibers of rats and mice. *Anat. Rec.* **167**, 379–387 (1970).
10. Elder, G.A. *et al.* Requirement of heavy neurofilament subunit in the development of axons with large calibers. *J. Cell Biol.* **143**, 195–205 (1998).
11. Maxwell, W.L. & Graham, D.I. Loss of axonal microtubules and neurofilaments after stretch-injury to guinea pig optic nerve fibers. *J. Neurotrauma* **14**, 603–614 (1997).
12. Stys, P.K. White matter injury mechanisms. *Curr. Mol. Med.* **4**, 113–130 (2004).
13. Reeves, T.M., Smith, T.L., Williamson, J.C. & Phillips, L.L. Unmyelinated axons show selective rostrocaudal pathology in the corpus callosum after traumatic brain injury. *J. Neuropathol. Exp. Neurol.* **71**, 198–210 (2012).
14. Iwata, A. *et al.* Traumatic axonal injury induces proteolytic cleavage of the voltage-gated sodium channels modulated by tetrodotoxin and protease inhibitors. *J. Neurosci.* **24**, 4605–4613 (2004).
15. Morrison, B., 3rd, Elkin, B.S., Dolle, J.P. & Yarmush, M.L. *In vitro* models of traumatic brain injury. *Annu. Rev. Biomed. Eng.* **13**, 91–126 (2011).
16. Lusardi, T.A., Rangan, J., Sun, D., Smith, D.H. & Meaney, D.F. A device to study the initiation and propagation of calcium transients in cultured neurons after mechanical stretch. *Ann. Biomed. Eng.* **32**, 1546–1558 (2004).
17. Mazzeo, A.T., Beat, A., Singh, A. & Bullock, M.R. The role of mitochondrial transition pore, and its modulation, in traumatic brain injury and delayed neurodegeneration after TBI. *Exp. Neurol.* **218**, 363–370 (2009).
18. Halestrap, A.P., McStay, G.P. & Clarke, S.J. The permeability transition pore complex: Another view. *Biochimie* **84**, 153–166 (2002).
19. Perry, S.W., Norman, J.P., Barbieri, J., Brown, E.B. & Gelbard, H.A. Mitochondrial membrane potential probes and the proton gradient: A practical usage guide. *BioTechniques* **50**, 98–115 (2011).
20. Dolle, J.P., Morrison, B., 3rd, Schloss, R.S. & Yarmush, M.L. An organotypic uniaxial strain model using microfluidics. *Lab Chip* **13**, 432–442 (2013).
21. Coronado, V.G. *et al.* Surveillance for traumatic brain injury-related deaths — United States, 1997–2007. *MMWR. Surveill. Summ.* **60**, 1–32 (2011).
22. Margulies, S.S., Thibault, L.E. & Gennarelli, T.A. Physical model simulations of brain injury in the primate. *J. Biomech.* **23**, 823–836 (1990).
23. Meaney, D.F. & Thibault, L.E. Physical model studies of cortical brain deformation in response to high strain rate inertial loading. In: *International Conference on the Biomechanics of Impacts, Lyon, France* (1990), pp. 215–224.

24. Morrison, B., 3rd, Meaney, D.F. & McIntosh, T.K. Mechanical characterization of an *in vitro* device designed to quantitatively injure living brain tissue. *Ann. Biomed. Eng.* **26**, 381–390 (1998).
25. Smith, D.H., Wolf, J.A., Lusardi, T.A., Lee, V.M. & Meaney, D.F. High tolerance and delayed elastic response of cultured axons to dynamic stretch injury. *J. Neurosci.* **19**, 4263–4269 (1999).
26. Vargas, M.E. & Barres, B.A. Why is Wallerian degeneration in the CNS so slow? *Annu. Rev. Neurosci.* **30**, 153–179 (2007).
27. Blumbergs, P.C. *et al.* Staining of amyloid precursor protein to study axonal damage in mild head injury. *Lancet* **344**, 1055–1056 (1994).
28. Toda, T. *et al.* Na^+/H^+ exchanger inhibitor cariporide attenuates the mitochondrial Ca^{2+} overload and PTP opening. *Am. J. Physiol. Heart Circ. Physiol.* **293**, H3517–3523 (2007).
29. Teshima, Y., Akao, M., Jones, S.P. & Marban, E. Cariporide (HOE642), a selective Na^+-H^+ exchange inhibitor, inhibits the mitochondrial death pathway. *Circulation* **108**, 2275–2281 (2003).
30. Rochlin, M.W., Wickline, K.M. & Bridgman, P.C. Microtubule stability decreases axon elongation but not axoplasm production. *J. Neurosci.* **16**, 3236–3246 (1996).
31. Reeves, T.M., Phillips, L.L. & Povlishock, J.T. Myelinated and unmyelinated axons of the corpus callosum differ in vulnerability and functional recovery following traumatic brain injury. *Exp. Neurol.* **196**, 126–137 (2005).
32. Wyss, J.M., Swanson, L.W. & Cowan, W.M. The organization of the fimbria, dorsal fornix and ventral hippocampal commissure in the rat. *Anat. Embryol.* **158**, 303–316 (1980).
33. Wolf, J.A., Stys, P.K., Lusardi, T., Meaney, D. & Smith, D.H. Traumatic axonal injury induces calcium influx modulated by tetrodotoxin-sensitive sodium channels. *J. Neurosci.* **21**, 1923–1930 (2001).
34. Hemphill, M.A. *et al.* A possible role for integrin signaling in diffuse axonal injury. *PloS One* **6**, e22899 (2011).
35. Van Vactor, D. Adhesion and signaling in axonal fasciculation. *Curr. Opin. Neurobiol.* **8**, 80–86 (1998).
36. Miledi, R. & Slater, C.R. On the degeneration of rat neuromuscular junctions after nerve section. *J. Physiol.* **207**, 507–528 (1970).
37. Lubinska, L. Early course of Wallerian degeneration in myelinated fibres of the rat phrenic nerve. *Brain Res.* **130**, 47–63 (1977).
38. Chaudhry, V., Glass, J.D. & Griffin, J.W. Wallerian degeneration in peripheral nerve disease. *Neurol. Clin.* **10**, 613–627 (1992).
39. Nicholls, D.G. & Budd, S.L. Mitochondria and neuronal survival. *Physiol. Rev.* **80**, 315–360 (2000).
40. Poppe, M. *et al.* Dissipation of potassium and proton gradients inhibits mitochondrial hyperpolarization and cytochrome c release during neural apoptosis. *J. Neurosci.* **21**, 4551–4563 (2001).
41. Sullivan, P.G., Thompson, M.B. & Scheff, S.W. Cyclosporin A attenuates acute mitochondrial dysfunction following traumatic brain injury. *Exp. Neurol.* **160**, 226–234 (1999).
42. Gergely, P., Jr. *et al.* Persistent mitochondrial hyperpolarization, increased reactive oxygen intermediate production, and cytoplasmic alkalinization characterize altered IL-10 signaling in patients with systemic lupus erythematosus. *J. Immunol.* **169**, 1092–1101 (2002).
43. Giovannini, C. *et al.* Mitochondria hyperpolarization is an early event in oxidized low-density lipoprotein-induced apoptosis in Caco-2 intestinal cells. *FEBS Lett.* **523**, 200–206 (2002).
44. Komary, Z., Tretter, L. & Adam-Vizi, V. Membrane potential-related effect of calcium on reactive oxygen species generation in isolated brain mitochondria. *Biochim. Biophys. Acta* **1797**, 922–928 (2010).
45. Suzuki, T., Ueno, H., Mitome, N., Suzuki, J. & Yoshida, M. F(0) of ATP synthase is a rotary proton channel. Obligatory coupling of proton translocation with rotation of c-subunit ring. *J. Biol. Chem.* **277**, 13281–13285 (2002).
46. Opii, W.O. *et al.* Proteomic identification of oxidized mitochondrial proteins following experimental traumatic brain injury. *J. Neurotrauma* **24**, 772–789 (2007).
47. Belzacq, A.S. *et al.* Bcl-2 and Bax modulate adenine nucleotide translocase activity. *Cancer Res.* **63**, 541–546 (2003).
48. Wennersten, A., Holmin, S. & Mathiesen, T. Characterization of Bax and Bcl-2 in apoptosis after experimental traumatic brain injury in the rat. *Acta Neuropathol.* **105**, 281–288 (2003).
49. Kruman, II & Mattson, M.P. Pivotal role of mitochondrial calcium uptake in neural cell apoptosis and necrosis. *J. Neurochem.* **72**, 529–540 (1999).
50. Ahmed, S.M., Rzigalinski, B.A., Willoughby, K.A., Sitterding, H.A. & Ellis, E.F. Stretch-induced injury alters mitochondrial membrane potential and cellular ATP in cultured astrocytes and neurons. *J. Neurochem.* **74**, 1951–1960 (2000).
51. Jayakumar, A.R. *et al.* Trauma-induced cell swelling in cultured astrocytes. *J. Neuropathol. Exp. Neurol.* **67**, 417–427 (2008).
52. Bernardi, P. & Petronilli, V. The permeability transition pore as a mitochondrial calcium release channel: A critical appraisal. *J. Bioenerg. Biomembr.* **28**, 131–138 (1996).
53. Masereel, B., Pochet, L. & Laeckmann, D. An overview of inhibitors of Na(+)/H(+) exchanger. *Eur. J. Med. Chem.* **38**, 547–554 (2003).
54. Ruiz-Meana, M. *et al.* Cariporide preserves mitochondrial proton gradient and delays ATP depletion in cardiomyocytes during ischemic conditions. *Am. J. Physiol. Heart Circ. Physiol.* **285**, H999–1006 (2003).
55. Villa-Abrille, M.C., Cingolani, E., Cingolani, H.E. & Alvarez, B.V. Silencing of cardiac mitochondrial NHE1 prevents mitochondrial permeability transition pore opening. *Am. J. Physiol. Heart Circ. Physiol.* **300**, H1237–1251 (2011).
56. Sullivan, P.G., Rabchevsky, A.G., Waldmeier, P.C. & Springer, J.E. Mitochondrial permeability transition in CNS trauma: Cause or effect of neuronal cell death? *J. Neurosci. Res.* **79**, 231–239 (2005).
57. Xu, M., Wang, Y., Ayub, A. & Ashraf, M. Mitochondrial K(ATP) channel activation reduces anoxic injury by restoring mitochondrial membrane potential. *Am. J. Physiol. Heart Circ. Physiol.* **281**, H1295–1303 (2001).
58. Troyan, M.B., Gilman, V.R. & Gay, C.V. Mitochondrial membrane potential changes in osteoblasts treated with parathyroid hormone and estradiol. *Exp. Cell Res.* **233**, 274–280 (1997).
59. Sullivan, P.G., Thompson, M. & Scheff, S.W. Continuous infusion of cyclosporin A postinjury significantly ameliorates cortical damage following traumatic brain injury. *Exp. Neurol.* **161**, 631–637 (2000).

SUPPLEMENTARY INFORMATION

CsA treated conditions

The effects of EIPA on axonal MMP were compared to those by cyclosporin A (CsA), a well known drug that targets the mitochondria and been shown to be neuroprotective during TBI[59]. The effects of CsA on MMP and axonal degeneration were assessed. CsA was administered at 1 μM in serum free media 1 hour before strain injury until the end of the experiment.

Immunohistochemical staining

Hippocampal slices and extending axons were fixed in 4% paraformaldehyde (Sigma) for 20 minutes. The cultures were washed three times in Tris Buffered Saline (TBS) (0.5M Tris Base, 9% NaCl, pH 7.4) for 5 minutes each, blocked and permeabilized for 1 hour at room temperature using 0.1% Triton-X, 1% bovine serum albumin, 10% goat serum and TBS. Primary antibodies in TBS with 1% goat serum were then added to cultures and incubated overnight at 4°C. After washing the cultures three times with TBS for 5 minutes each, secondary antibodies in TBS were added for 1 hour at room temperature. The cultures were then washed three times with TBS for 5 minutes each and stored in PBS at 4°C for imaging. Primary antibodies used were: mouse anti-tubulin beta III IgG1 (Millipore) at 10 μg/ml and rabbit anti-amyloid precursor protein (APP) C-terminus IgG (Millipore) at 10 μg/ml. Secondary antibodies used were: goat anti-mouse Alexa Fluor 647 IgG (Invitrogen) and goat anti-rabbit Alexa Fluor 488 IgG (Invitrogen). Isotype controls used were: purified mouse IgG1 (BD Bioscience) at 10 μg/ml and purified rabbit IgG (Invitrogen) at 10 μg/ml. Axons were excited using 488 nm and 647 nm filters and the same exposure time for each filter was used for all experiments.

Supplementary Table 1 Increase in the number of mitochondria by 24 hours after 25% applied strain as compared to before injury. *P < 0.05 positions 1, 2 and 11 are significant compared to positions 4–7, and all positions were significant as compared to before injury (number of experiments = 6).

	Position across pressure cavity										
	1	2	3	4	5	6	7	8	9	10	11
	*	*									*
Fold increase	3.9 ± 0.5	3.1 ± 0.4	2.8 ± 0.5	2.1 ± 0.4	2.2 ± 0.4	2.1 ± 0.4	2.4 ± 0.3	2.4 ± 0.6	2.4 ± 0.7	2.8 ± 0.5	3.3 ± 0.5

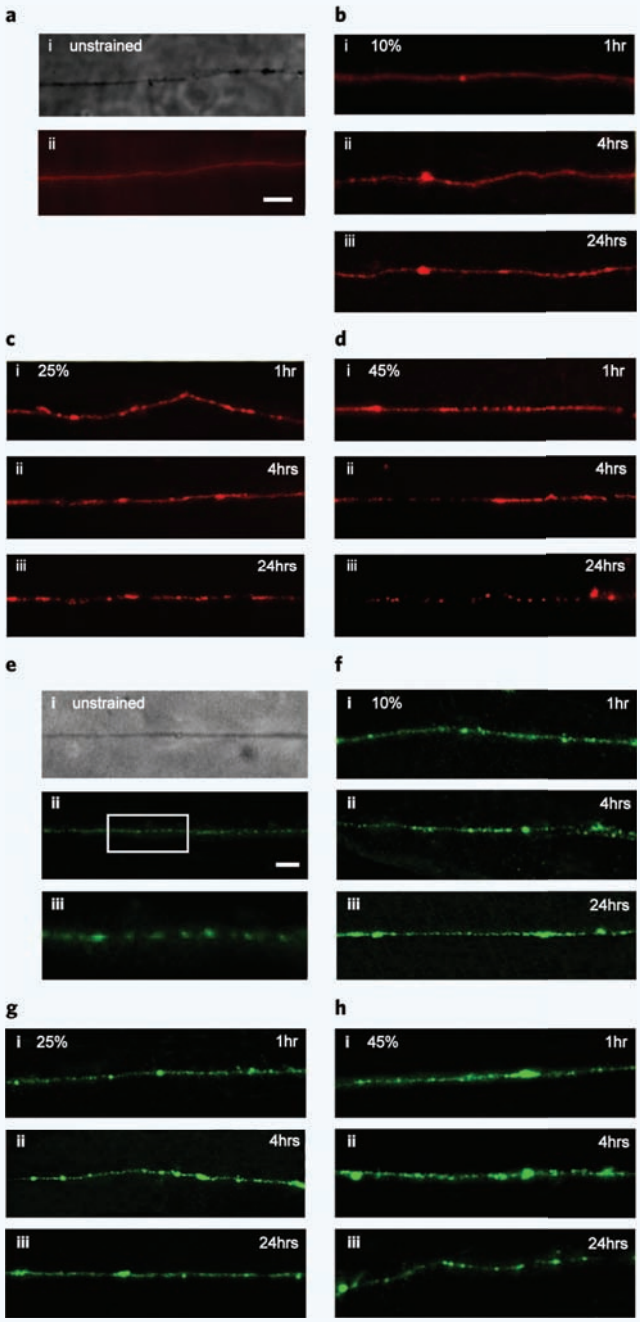

Supplementary Figure 1 Representative images of strain injured axons immunostained for β-tubulin and amyloid precursor protein (APP). β-tubulin staining: (**a**) Unstrained axon, (i) phase contrast image and (ii) β-tubulin stain; (**b**) 10% applied strain, (i) 1 hour post injury, (ii) 4 hours post injury and (iii) 24 hours post injury; (**c**) 25% applied strain, (i) 1 hour post injury, (ii) 4 hours post injury and (iii) 24 hours post injury; (**d**) 45% applied strain, (i) 1 hour post injury, (ii) 4 hours post injury and (iii) 24 hours post injury. APP staining: (**e**) Unstrained axon, (i) phase contrast image, (ii) APP staining and (iii) enlarged box section of (ii); (**f**) 10% applied strain, (i) 1 hour post injury, (ii) 4 hours post injury and (iii) 24 hours post injury; (**g**) 25% applied strain, (i) 1 hour post injury, (ii) 4 hours post injury and (iii) 24 hours post injury; (**h**) 45% applied strain, (i) 1 hour post injury, (ii) 4 hours post injury and (iii) 24 hours post injury. Scale bar, 10 μm.

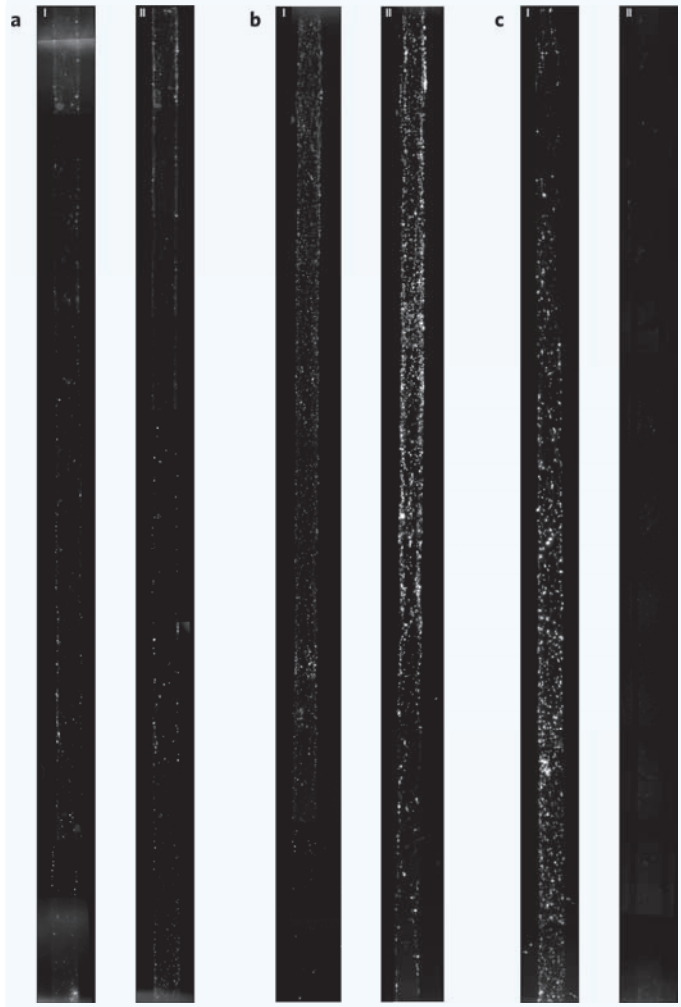

Supplementary Figure 2 Representative images of changes in MMP after applying a uniaxial strain injury as assessed using JC-1 dye. (**a**) 10% applied strain, (i) JC-1 fluorescence before injury and (ii) 24 hours after injury. (**b**) 25% applied strain, (i) JC-1 fluorescence before injury and (ii) 24 hours after injury. (**c**) 45% applied strain, (i) JC-1 fluorescence before injury and (ii) 24 hours after injury.

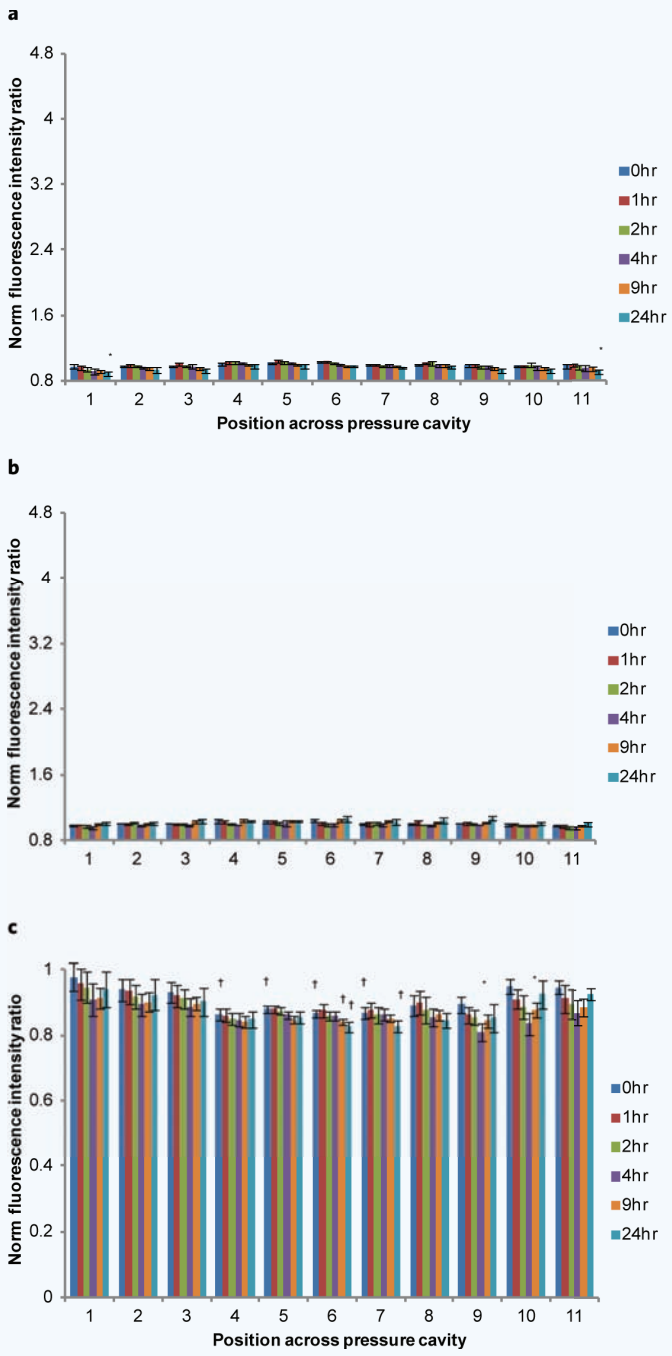

Supplementary Figure 3 Monitoring mitochondrial membrane potential changes over a 24-hour period after application of Cyclosporin A and uniaxial strain injuries. Mitochondrial membrane potential changes are normalized to their potential before injury and assessed at 11 discrete sections along the axons and 6 time points, i.e. immediately following injury (0 hour), 1 hour, 2 hours, 4 hours, 9 hours and 24 hours post injury. (**a**) 10% applied strain, (**b**) 25% applied strain and (**c**) 45% applied strain. *$P < 0.05$ compared to MMP at that particular position before injury. †$P < 0.05$ compared to MMP at that particular time point at positions 1 and 11 (number of experiments = 6).

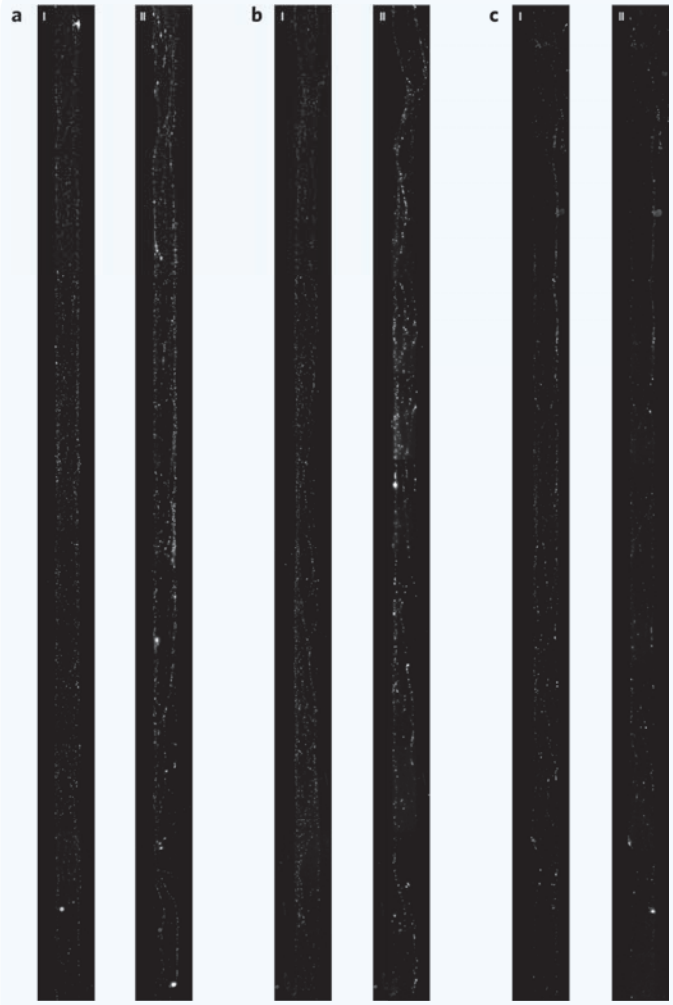

Supplementary Figure 4 Representative images of changes in MMP after application of the NHE-1 inhibitor EIPA and uniaxial strain injuries as assessed using JC-1 dye. (**a**) 10% applied strain, (i) JC-1 fluorescence before injury and (ii) 24 hours after injury. (**b**) 25% applied strain, (i) JC-1 fluorescence before injury and (ii) 24 hours after injury. (**c**) 45% applied strain, (i) JC-1 fluorescence before injury and (ii) 24 hours after injury.